Indoles from Alkynes and Aryl Azides. Scope and Theoretical Assessment of Ruthenium Porphyrin-Catalyzed Reactions

Daniela Intrieri,[a] Daniela Maria Carminati,[b] Paolo Zardi,[c] Caterina Damiano,[a] Gabriele Manca,*[d] Emma Gallo*[a] and Carlo Mealli[d]

Abstract: A symbiotic experimental/computational study analyzed the Ru(TPP)$(NAr)_2$-catalyzed *one-pot* formation of indoles from alkynes and aryl azides. Thirty different C_3-substituted indoles were synthesized and best performances, in term of yields and regioselectivities, were observed by reacting ArC≡CH alkynes with 3,5-$(EWG)_2C_6H_3N_3$ azides, whilst the reaction was less efficient by using electron-rich aryl azides. A DFT analysis describes the reaction mechanism in terms of the energy costs and orbital/electronic evolutions; the limited reactivity of electron-rich azides was also justified. In summary, PhC≡CH alkyne interacts with one NAr imido ligand of Ru(TPP)$(NAr)_2$ to give a residually dangling C(Ph) group which, by coupling with a C(H) unit of the *N*-aryl substituent, forms a 5+6 bicyclic molecule. In the process, two subsequent spin changes allow inverting the conformation of the sp^2 C(Ph) atom and its consequent electrophilic-like attack to the aromatic ring. The bicycle isomerizes to indole *via* a two-steps outer sphere H-migration. Eventually, a 'Ru(TPP)(NAr)' *mono*-imido active catalyst is reformed after each azide/alkyne reaction.

Introduction

The indole ring represents one of the most active pharmacophores in Nature, which confers to indole-containing molecules a plethora of biological and/or pharmaceutical features.[1] The molecular skeleton of several naturally-occurring and clinically employed molecules shows an indole motif, which is responsible for anti-hypertensive, anti-inflammatory, anti-tumor, anti-migraine, anti-cholesterol and many other pharmacological activities (Figure 1).[2]

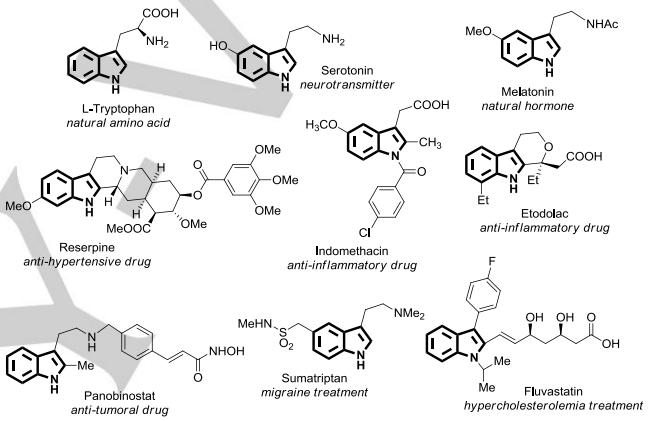

Figure 1. Selected examples of bioactive and pharmaceutical indole-containing compounds.

Since the publication of the pioneering Fischer's synthesis of indoles,[3] a great attention has always been devoted to design efficient strategies to synthesize[4] and functionalize[5] indoles. Although many metal-free procedures have successfully been applied,[6] transition metal catalyzed-methodologies have emerged as more attractive methods due their capability in controlling the selectivity and conditions of the processes.[7] In order to optimize the performance of the methodology without affecting the process eco-sustainability, reaction components are rigorously selected, and either *ortho*-disubstituted or *mono*-functionalized aromatic compounds have been found to represent valuable starting materials. Even if *ortho*-disubstituted[8] species are reagents of choice in several synthetic procedures (Figure 2a), their use often requires time-consuming pre-functionalization steps thus, the employment of *mono*-substituted aromatic reactants is constantly increasing. *Mono*-substituted species can be efficiently transformed into indoles through C-H bond activation reactions[4a, 9] and many synthetic procedures, which employ *N*-aryl enamines[10], *N*-aryl imines,[11] nitroarenes,[12] nitrosoarenes,[13] anilines,[14] anilides[15] as the starting materials, have been reported up to now (Figure 2b).

[a] PhD D. Intrieri, Dr. C. Damiano, Prof. E. Gallo
Department of Chemistry
University of Milan
Via Golgi 19, I-20133 Milan
E-mail: emma.gallo@unimi.it
[b] PhD D. M. Carminati,
Department of Chemistry
University of Rochester
416 Hutchison Hall, NY 14627-0216
[b] PhD P. Zardi
Department of Chemical Sciences
University of Padua
Via F. Marzolo 1, I-35131 Padua
[b] PhD G. Manca, Dr. C. Mealli
Istituto di Chimica dei Composti OrganoMetallici
ICCOM-CNR
Via Madonna del Piano 10, I-50019 Sesto Fiorentino
E-mail: gabriele.manca@iccom.cnr.it

Supporting information for this article is given via a link at the end of the document.

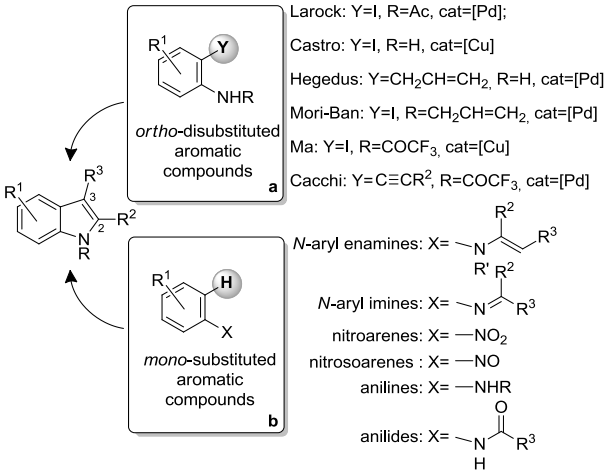

Figure 2. Selection of *ortho*-disubstituted and *mono*-substituted aromatic reagents.

Indoles can be also obtained by ring-closure reactions of aryl azides (ArN_3),[16] which are a sustainable and atom-efficient class of aminating agents thanks to the formation of benign N_2 as the only by-product of the annulation process. The catalytic performance of this class of molecules is due to the formation of a very reactive nitrene intermediate 'ArN' which is responsible for amination reactions.[16c] Figure 3 shows the most relevant azide molecules which have been employed for the catalytic *intra*molecular synthesis of indoles.

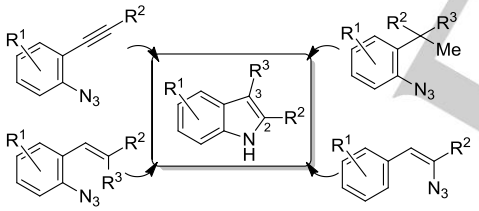

Figure 3. Selection of aryl azides employed for the synthesis of indoles.

During our ongoing studies on the use of aryl azides as nitrene sources, we discovered that azides are very reactive towards alkynes in forming indoles rather than triazoles in the presence of ruthenium porphyrin complexes. In our previous communication,[17] we reported the one-pot synthesis of differently substituted indoles (Scheme 1) thus, in view of the interest in developing sustainable methods for achieving such valuable fine-chemicals, the catalytic activity of ruthenium porphyrins was further investigated. Note that to the best of our knowledge, only one other example was recently published on the reaction of sulfonyl azide with isocyanides yielding 3-imine indoles by an *inter*molecular mechanism.[18]

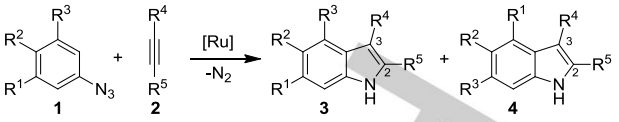

Scheme 1. General scheme of ruthenium porphyrin-catalyzed synthesis of indoles from aryl azides and alkynes.

In addition to the study of the reaction scope, a mechanistic study, based on the availability of many experimental and theoretical data, added rich information on the evolution of the reaction mechanism that involves both the *inner* and *outer* sphere of the catalyst. Thus, the paper clarifies various key aspects of the intriguing reactivity also providing important suggestions for the process optimization.

Results and Discussion

Study of the Reaction Scope

As previously communicated,[17] the comparison of the catalytic efficiency of different ruthenium porphyrins in promoting the model reaction of 3,5-*bis*(trifluoromethyl) phenyl azide (**1a**) with phenylacetylene (**2a**) pointed out that ruthenium *bis*-imido Ru(TPP)$(NAr)_2$ (**5**) (TPP = dianion of tetraphenyl porphyrin, Ar = 3,5-$(CF_3)_2C_6H_3$) complex[19] performed the best. The optimization of the experimental conditions allowed us obtaining differently C_3-substituted indoles in high yields and short reaction times. The catalytic activity of **5** was then further investigated and new obtained data are here discussed together with those already reported in our communication[17] for providing a more complete scenario on the applicability of the synthetic methodology.

The efficiency of complex **5** was first investigated by reacting several substituted azides with phenylacetylene (**2a**), and resulted data are showed in Table 1. The indole formation occurs by the activation of the C-H bond[17] which is placed onto the *ortho* position with respect to the N_3 functionality of the starting azide. The presence of electron withdrawing groups (EWG_s) on *meta* positions of azide had a positive effect on the reaction productivity while, when electron-rich 3-^{t}Bu-phenyl azide, 4-^{t}Bu-phenyl azide and 3,4,5-trimethoxyphenyl azide were reacted with **2a**, the formation of corresponding indoles was not observed (vide infra for the rationalization of this effect).

Considering that the ring-closing reaction yielding indoles involves one of the two C-H bonds adjacent to the N_3 group, isomers **3** and **4** (Scheme 1 and Table 1) can both be formed in a ratio which depends on the electronic nature of azide substituents. Clearly, the use of 3,5-disubstited azides, with $R^1 = R^3$, resulted in the formation of only one regiosomer due to the chemical equivalence of the two aromatic C-H bonds. The reaction of either 3,5-$(CF_3)_2C_6H_3N_3$ (**1a**) or 3,5-$(NO_2)_2C_6H_3N_3$ (**1b**) with **2a** afforded corresponding **3aa** and **3ba** indoles in very good yields (86% and 82%, respectively) and short reaction times (1.0 h and 0.5 h, respectively).

Table 1. Complex **5**-catalyzed synthesis of indoles **3** and **4** from **2a** and aryl azides **1a-g**.[a,b]

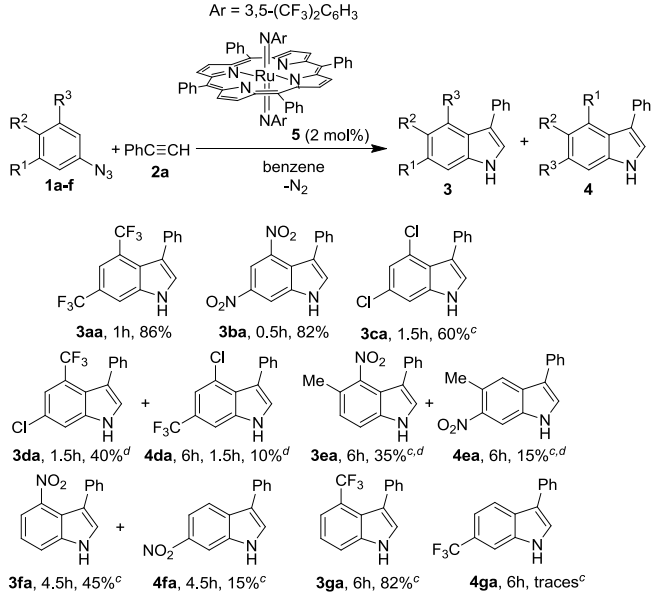

[a] Catalyst **5** (0.01 mmol) in 10.0 mL of refluxing benzene under N_2, mol ratio **5**/azide/**2a** = 1:50:250. [b] Isolated yield. [c] Ref 17. [d] Mol ratio **5**/azide/**2a** = 1:50:1000. [e] NMR yield calculated in the **3**/**4** mixture.

The high regioselectivity of the reaction was proved by the formation of C_3-substituted isomer as the sole reaction product, not traces of C_2-substituted indole were obtained. It is important to underline that when **1b** azide was employed as the reactant, the corresponding **3ba** indole precipitated from the reaction mixture and the desired product was isolated in a pure form by a simple filtration at the end of the catalytic reaction. This convenient work-up of the reaction rendered the procedure more sustainable because any other expensive and time-consuming purification procedures, such as flash chromatography, were not required. The reaction of 3,5-$(Cl)_2C_6H_3N_3$ (**1c**) with **2a** formed **3ca** indole in a 60% yield pointing out that the reaction efficiency decreases by decreasing the electron withdrawal power of azide substituents.

Both **3** and **4** indole isomers were obtained either when two different substituents were present onto the 3 and 5 positions of the azide or 3,4-disubstituted aryl azides were employed as starting materials, due to the presence of two chemically inequivalent C-H aromatic bonds nearby the N_3 moiety. The reaction of 3-(CF_3)-5-$(Cl)C_6H_3N_3$ (**1d**) or 3-(NO_2)-4-$(Me)C_6H_3N_3$ (**1e**) azides with **2a** yielded indoles **3da** and **3ea** as the most abundant isomers suggesting that the reaction pathway favors the formation of indoles which bear the most electron withdrawing group on the 4 position of the heterocycle. The 4-substituted indoles **3fa** and **3ga** were also obtained, as principal isomers, when either 3-$(NO_2)C_6H_4N_3$ (**1f**) or 3-$(CF_3)C_6H_4N_3$ (**1g**) azides were employed as the reagents. Even if, an electron withdrawing R^3 substituent (CF_3 or NO_2 group) can activate C-H bonds which are located either in *ortho* or *para* position referring to R^3, achieved data indicated that the cleavage of an *ortho* C-H bond was always favored. The high directing capability of CF_3 permitted the formation of **3ga** indole in 82% yield and **4ga** isomer was only formed in small amounts (5% yield), as revealed by GC-MS and ^{19}F NMR analyses. The worse regioselectivity, which was observed when **1f** azide reacted with **2a** to form a **3fa**/**4fa** mixture, was ascribed to the mesomeric effect of the nitro group.

Then, in order to enlarge the reaction scope, the most reactive and selective 3,5-disubstituted aryl azides **1a** and **1b** were reacted with terminal aromatic alkynes **2b**-**n** (Table 2).

Table 2. Synthesis of indoles of type **3** from the **5**-catalyzed reaction of aryl azides (**1a-b**) with alkynes (**2b-n**).[a,b]

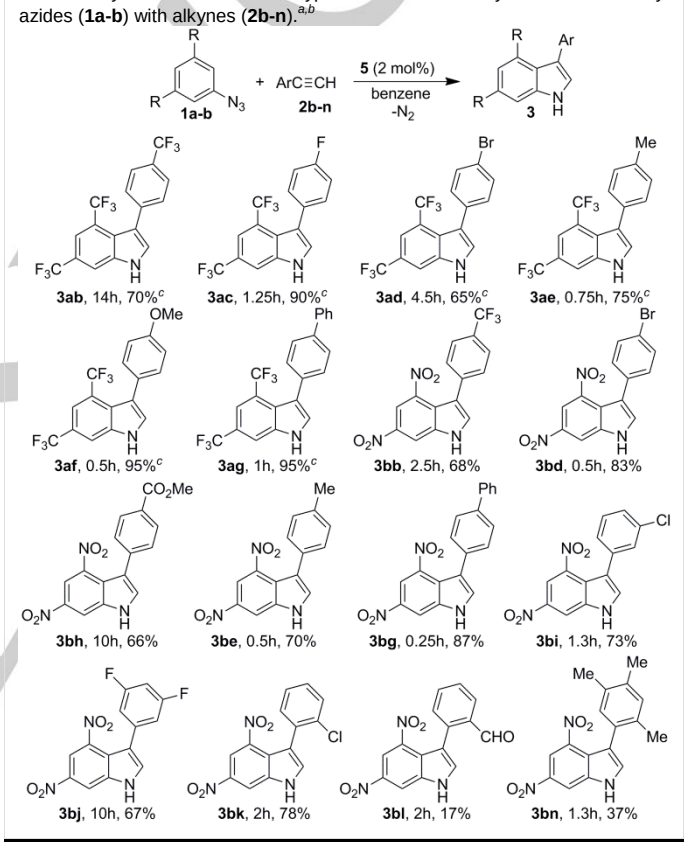

[a] Catalyst **5** (0.01 mmol) in 10.0 mL of refluxing benzene under N_2, mol ratio **5**/azide/alkyne = 1:50:250. [b] Isolated yield. [c] Ref 17.

Achieved results suggest a modest dependence of the reaction productivity on electronic characteristics of the employed alkyne. Even if, similar indole yields were observed by using both electron-rich and electron-poor alkynes in the reaction with **1a** or **1b**, in many cases shortest reaction times (see Experimental Section for details) were achieved by employing alkyne reagents bearing an electron donating group (EDG) onto the *para* aromatic position (e.g. compare **3ae**, **3af**, **3be** with **3ab**, **3ad**, **3bh**, Table 2).

Conversely to the observed low electronic effect, the steric hindrance of alkynes influenced the reaction productivity to a greater extent. Even if *mono*-substituted alkynes were efficiently

converted into corresponding indole independently for the position where the substituent was placed (**3bi** and **3bk**, Table 2), the presence highly substituted aryl alkyne moiety was responsible for a decrease of the reaction yield; the reaction of **1b** with the sterically hindered 2,4,5-$(Me)_3C_6H_2C{\equiv}CH$ (**2n**) species yielded the corresponding indole **3bn** in the low 37% yield (Table 2). The procedure did not tolerate the presence of reactive functional groups such as an aldehyde and the reaction of **1b** with **2l** yielded indole **3bl** in a very low yield (17%) due to the formation of several side-products which were not identified.

It is important to remind that all the indoles (**3bb**, **3bd**, **3bh**, **3be**, **3bg**, **3bi**, **3bj**, **3bk**, **3bl**, **3bn**, Table 2) which were obtained by using 3,5-$(NO_2)_2C_6H_3N_3$ (**1b**) as the precursor, were directly collected from the reaction mixture by a simple filtration.

Finally, we studied the reactivity of internal alkynes PhC≡CPh (**2o**) and PhC≡CMe (**2p**) towards **1a** or **1b** azides but unfortunately, the synthesis of indoles **3ao**, **3ap** and **3bo** (Table 3) occurred in low yields and long reaction times due to the steric hindrance of starting alkynes (see Experimental Section). Even if a modest productivity was always registered, only the isomer which bears the more sterically hindered phenyl group on the C_3 position of the heterocycle, was isolated. Similar results were obtained by reacting $CO_2EtC{\equiv}CH$ (**2q**) with **1a** where the desired indole **3aq** was isolated after 13 hours in the very low yield of 13%. The methodology was ineffective when aliphatic alkynes, such as trimethylsilyl acetylene or 1 heptyne, were the selected reagents.

Table 3. Complex **5**-catalyzed synthesis of indoles from alkynes **2o-q** and aryl azides **1a** or **1b**.[a,b]

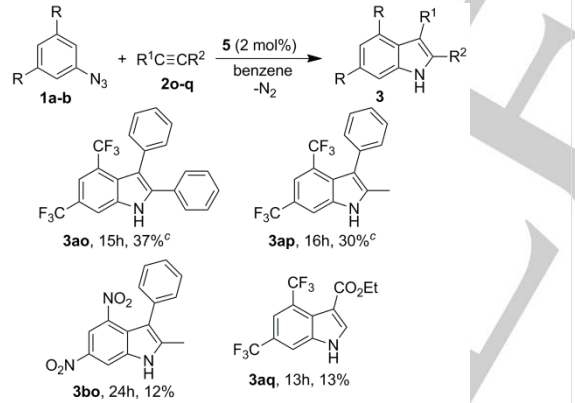

[a] Catalyst **5** (0.01 mmol) in 10.0 mL of refluxing benzene under N_2, mol ratio **5**/azide/alkyne = 1:50:250. [b] Isolated yield. [c] Ref 17.

Considering the good affinity of ruthenium for oxygen-containing species, the reduced catalytic performances, observed when alkynes **2l** (Table 2) and **2q** (Table 3) were employed, can be due to the coordination of the alkyne C=O group to ruthenium atom, which causes the catalyst deactivation. This hypothesis was supported by the decomposition of Ru(TPP)$(NAr)_2$ (**5**) that was observed when **5** was reacted with the sole **2l** by using the experimental conditions reported in Table 2.

It should be noted that, as previously reported,[20] ruthenium porphyrin catalysts can promote the insertion of the nitrene functionality of an aryl azide into the C_2-H bond of an indole leading the C_2-iminated product. Thus, in order to favor the conversion of the azide into corresponding indole with respect to the C_2-imination side-reaction, an alkyne excess was always employed.

In summary, the study of the reaction scope disclosed that the procedure is highly effective for producing indoles from electron-poor azides and terminal aromatic alkynes whilst, the reaction efficiency dropped by using either electron-rich azides or internal as well as aliphatic alkynes. Then, in order to examine the power and limitations of the synthetic procedure, the catalytic mechanism was investigated by both experimental and computational analyses.

Mechanistic Investigation

In order to study the reaction mechanism, some experiments were performed and reported in our previous communication.[17] A summary of those data is listed in the following (see SI for experimental details): i) Indole isn't formed by a rearrangement process of a triazole molecule, which can be obtained by the free-catalysts reaction of alkyne with azide. In fact, no reaction was observed by treating catalyst **5** with a 4:1 mixture of 1-(3,5-*bis*(trifluoromethyl)phenyl)-5-phenyl-1*H*-1,2,3-triazole and 1-(3,5-*bis*(trifluoromethyl)phenyl)-4-phenyl-1*H*-1,2,3-triazole to exclude a possible metal-catalyzed transformation of triazole into indole by N_2 release. ii) The imido "NAr" moiety of Ru(TPP)$(NAr)_2$ (**5**) can be directly transferred to the alkyne substrate, as supported by the stoichiometric reaction between **5** and phenylacetylene (**2a**) which yielded indole **3aa** (Table 1) in 50% yield. iii) The analysis of the reaction between phenylacetylene-*d* (PhC≡CD) and **1a** revealed that the C_2 position of the obtained indole was occupied by a deuterium atom to indicate that the C-D alkyne bond is not broken during the annulation reaction. As a consequence, a hydrogen-transfer (HAT) reaction should occur from the aromatic C-H bond of azide to indole nitrogen atom to form the NH bond. iv) The cleavage of the aromatic C-H bond does not represent the rate-determining step of the catalytic cycle, as suggested by the lack of an appreciable isotopic effect (k_H/k_D = 1.1) in the reaction of **2a** with an equimolar amount of **1a** and its deuterated 3,5-$(CF_3)_2C_6D_3N_3$ derivative; v) The participation of radical mechanisms can be excluded since **3aa** was formed in comparable rates both in in the absence and in the presence of the radical trapping agent TEMPO (2,2,6,6-tetramethylpiperidin-1-yl)oxy).

On the basis of experimental results described above and literature data, which report the formation of unstable antiaromatic 1*H*-azirines[6, 21] from the reaction of nitrenes with acetylenes as well as the transformation of 2*H*-azirines into indoles,[22] we hypothesized[17] the initial formation of a metastable three-membered ring. The potential mechanism to transform *N*-aryl-1*H*-azirine into the desired indole **3aa**, possibly involving a ring-opening reaction, is presented in Scheme 2. Unfortunately, no spectroscopic evidence supports the formation of the mentioned azirine intermediate, hence any hint on the feasibility of the process may emerge from an *in silico* analysis. The corresponding details, reported in a section of the SI, seem to exclude such a possibility

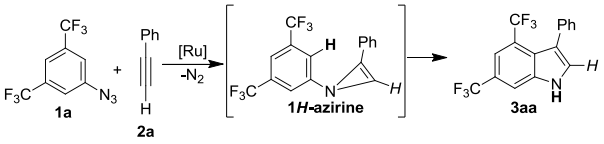

Scheme 2. Proposed pathway of the indole formation by a ring-opening reaction of a putative *N*-aryl-1*H*-azirine.

Kinetic Study.

The kinetic study of the **5**-catalyzed indole formation was undertaken by using the model reaction between 3,5-*bis*(trifluoromethyl)phenyl azide (**1a**) and phenylacetylene (**2a**). First, the consumption of aryl azide was followed by IR spectroscopy by monitoring the decrease of the intensity of the **1a** absorption (A) at 2116 cm^{-1} in the reaction where the **5**/azide/alkyne ratio of 2:50:250 was employed (see SI for experimental details). Since the reaction was run in the presence of a large **2a** excess (*pseudo* zero-order in alkyne), the linear fit of ln(A/Ao) (A = IR absorbance at each measure; Ao = initial IR absorbance) *versus* time indicated a first-order dependence of the reaction with respect to azide **1a** concentration (Figure 4a) and that no relevant catalyst deactivation occurred during the reaction.

The kinetic order of the reaction rate with respect to catalyst **5** concentration was investigated by repeating the experiment described above in the presence of different amounts of the catalyst. A first-order dependence on azide concentration was always observed for each kinetic run (see SI) and the values of the observed kinetic constants (k_{obs}) show a linear dependence on the catalyst concentration (Figure 4b), indicating that the reaction is also first-order in **5**. This rules out any mechanistic proposal in which either the porphyrin dimer formation or any reaction involving more than one "Ru(TPP)" unit is involved.

The kinetic order with respect to the alkyne **2a** was finally investigated by recording the rate of a series of reactions run at a constant catalyst concentration and a variable concentration of the alkyne, which was always large enough to ensure that a *pseudo* zero-order rate with respect to this reagent would be observed. The observed first-order kinetic constants again varies linearly with the alkyne concentration (Figure 4c, see SI for a plot of all individual reaction profiles), proving that the reaction rate is also first order in **2a**.

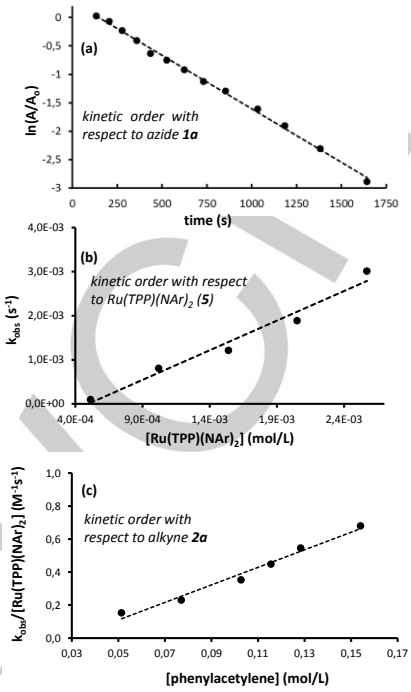

Figure 4. Kinetic dependence of the reaction rate with respect to **1a** (*a*), **5** (*b*) and **2a** (*c*) concentrations.

Thus, the kinetic equation describing the reactions can be formulated as $-d[azide]/dt = k'_{obs}[Ru(TPP)(NAr)_2][azide][alkyne]$. Since a trimolecular reaction can be excluded, a kinetic equation of this kind implies that two of the reaction components must be involved in a reversible interaction during the cycle. Considering that **1a** and **2a** do not form indole **3aa** in a free-metal reaction[17] and that triazoles cannot be transformed into indole in the presence of the ruthenium catalyst (see above), kinetic data indicates that either azide or alkyne should reversibly coordinate the ruthenium catalytically active species **A** to give either species **B** or **D**, as shown by the alternative *path a* or *path b* in Scheme 3. It is important to note that the observed first-order with respect to the catalyst **5** excludes a possible reaction between species **B** and **D**, in which both reagents are activated by the metal coordination. In fact, in this latter case a bimetallic pathway should result in a second-order dependence with respect to the catalyst concentration. The **B** or **D** adducts cannot be experimentally detected because the reaction equilibrium should be shifted to the left, towards the side of the azide and alkyne reagents.

The two alternative mechanisms of the reaction between phenylacetylene (but also another alkyne) and substituted aryl azides (*path a* and *path b* of Scheme 3) differ for the inverted order of the interaction between the ruthenium species and the two involved reagents, with no distinction emerging from kinetics.

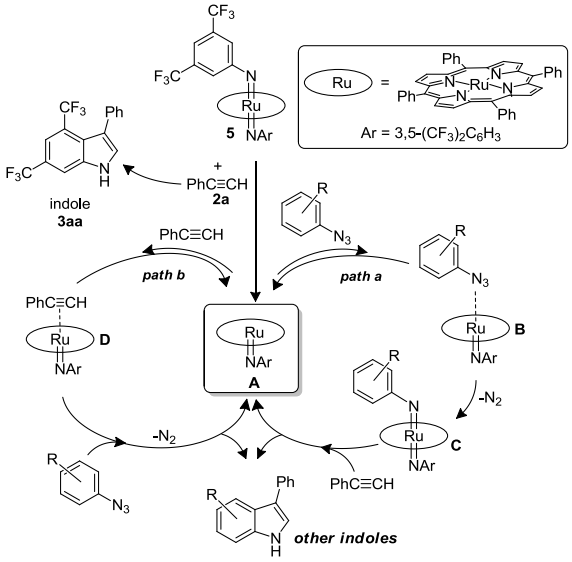

Scheme 3. Ru-catalyzed indole formation.

The very first step of Scheme 3 is the general stoichiometric reaction between complex **5** and phenylacetylene **2a** giving indole **3aa**, as a sacrificial side-product. Due to the presence of two 3,5-$(CF_3)_2C_6H_3N$ imido moieties as axial ligands of catalyst **5**, the formation of active species **A** is inevitably accompanied by the release of one equivalent of **3aa**, independently from the employed azide reactant. This side-reaction can be neglected in view of the very low amount of **3aa** (stoichiometric ratio with respect to **5**), which can be easily separated from the target indole corresponding to the employed azide and alkyne reactants. Similarly, the formation of **1a**-derived indole is not a drawback in all the indole syntheses here reported.

A detailed analysis of the reaction between **5** and **2a** is highly educational because implies the mechanistic underpinnings of the whole catalytic cycle. The mentioned step generates the *mono*-imido species **A** that is potentially the active catalyst for either the cycle *a* or *b*, depending on the first formed intermediate **B** or **D** (Scheme 3).

Analogously to other similar mechanisms of nitrene transfer reactions mediated by ruthenium imido complexes,[23] intermediate **B** can easily lose N_2 to form *bis*-imido complex **C**, which could positively interact with alkyne yielding the desired indole (Scheme 3, *path a*). Conversely, the dihapto coordination of alkyne **2a** to **A** would lead to intermediate **D** that may interact with an azide also giving the final indole product (Scheme 3, *path b*). In order to shed some light on the mechanism of the indole formation, a systematic DFT study was performed.

Electronic Underpinnings of the indole formation mechanism based on DFT calculations

The potential pathways presented in Scheme 3 represent a useful guideline for the study of the reaction mechanism. Many of the proposed steps are corroborated by computing the evolution of the stereochemical, electronic and energetic features. Unprecedented aspects of the chemical reactivity emerge, such as a spin state change of the system, which suitably rearranges the stereochemistry to allow the C-C coupling, hence the formation of the bicyclic molecule (see below).

Questionable reliability of *path b* in Scheme 3. The *mono*-imido complex **A** is common to the two foreshadowed pathways. *Path b* suggests the dihapto coordination of the alkyne to the metal to give complex **D**, which would couple with one azide reactant, allowing the ring-closing reaction to indole. Although complex **D** could be fully optimized (see Figure S18), the feasibility of *path b* could not be further corroborated, as discussed in the SI.

Details of the more probable catalytic formation of indole through *path a*. A definitely more realistic computational evidence emerged on the evolution of the system through *path a* of Scheme 3. In fact, all the important intermediates, transition states (TS) and products were fully characterized, thus allowing the determination of reasonable profiles from both the stereochemical and energetic viewpoints. It emerged that the process evolves thanks to the attainment of intermediates of variable spin multiplicity.

The experimental Ru(TPP)$(NAr)_2$ catalyst **5** plus all the reactants sum up to > 100 atoms, hence all the computational models, characterized by the letter **m**, have been slightly simplified. The used porphine ligand has H atoms in place of the *meso*-aryl substituents of the experimentally used porphyrin and one of the two imido ligands is as simple as NMe in the *bis*-imido model [Ru](NMe)(NAr) ([Ru] = Ru(porphine), Ar = 3,5-$(CF_3)_2C_6H_3$), whose optimized ground state structure (singlet $\mathbf{5m_S}$) is shown in Figure 5.

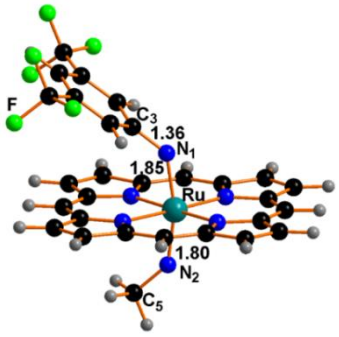

Figure 5. Optimized structure of *bis*-imido singlet complex [Ru](NMe)(NAr) ($\mathbf{5m_S}$).

Its subsequent reaction with PhC≡CH (**2a**) and the following steps were computationally monitored up to the release of the indole product **3aa**. At this point, the residual *mono*-imido fragment [Ru](NMe) (**Am**) becomes the fundamental catalyst, as it activates a new **1a** azide molecule and regenerates the precursor $\mathbf{5m_S}$ through a series of subsequently described steps. The reliability of $\mathbf{5m_S}$ as a model catalyst was corroborated by a satisfactory comparison with a known experimental structure.[19b] In our model, the 0.05 Å difference between the two Ru-N axial

distances suggests a possible steric hindrance between the aryl substituent of the imido moiety and the porphine macrocycle. Also remarkable are the bent and eclipsed N-C bonds (N_1-C_3 and N_1-C_5, Figure 5) of the two imido ligands, whose plane is staggered with respect to any Ru-N_{eq} linkage. Any deviation from the given arrangement plays a key role in the tuning of the reactivity.

Basic π electron interactions in the *bis*-imido complex. The MO description of the delocalized MeN=Ru=NAr $\pi_\perp$ and $\pi_\parallel$ systems in Scheme 4 is helpful to interpret the overall electronic evolution.

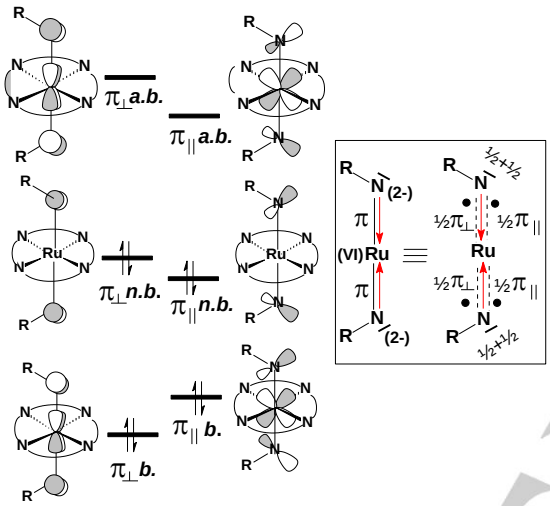

Scheme 4. Delocalized $\pi_\perp$ and $\pi_\parallel$ sets of interactions in a *bis*-imido [Ru] diamagnetic complex with the implications for the structural formulas appearing in the box (σ bonds in red).

None of the three sets of double levels is exactly degenerate due to the bending of the two imido ligands in one plane. Overall the diagram depicts the basic NR(p_π)/Ru(d_π) interactions, while the role of the porphine π levels is in first approximation excluded. A combination of delocalized imido lone pairs ($\pi_\perp$*n.b.* and $\pi_\parallel$*n.b.*) lies in between the bonding and antibonding levels, namely $\pi_\perp$*b.*+ $\pi_\parallel$*b.* and $\pi_\perp$*a.b.*+ $\pi_\parallel$*a.b.*, respectively. The MO diagram contains a total of 8 electrons, four of which are attributed to the Ru(II) filled d_{xz}+d_{yz} orbitals, while the other four belong to the two NR imido ligands. Such a picture also emerged in our previous studies of the azide activation by [Ru], where the departing N_2 leaves $2e^-$ at the coordinated NR grouping.[23c] The available Ru d_π electrons preferentially localize at the *trans*-axial N atoms for electronegativity reasons, thus formally implying an oxidized Ru(VI) ion and two dianionic imido ligands. The >60% Ru character of the highest $\pi_\parallel$*a.b.* and $\pi_\perp$*a.b.* vacant levels corroborates the existence of two Ru=N *trans*-axial double bonds, as indicated by the first structural formula in the box of Scheme 4. In actuality, the latter picture is better described by four half π bonds with $1e^-$ in each case, associated to two dative N→Ru σ linkages (red arrows). Incidentally, the MO π picture of Scheme 4 recalls that of the much simpler linear triatomic CO_2[24] where eight delocalized π electrons determine four half π bonds, normally depicted as two consecutive double ones.[25] Also, the known R-N=C=N-R carbodiimide, which is additionally relevant for its reactivity with group 4 and 5 imido complexes,[26] compares with **5m$_S$** for the similarly bent NR groups.[27]

Also due to the delocalization of the π electrons in **5m$_S$**, the *in plane* σ donor power of any imido sp^2 hybrid is limited, but still appropriate for the interaction with the incoming alkyne (see below). On the other hand, *bis*-imido complexes are also known to promote diradical reactivity, as in the case of the allylic amination and aziridination of unsaturated alkenes by azides.[23c, 28] For instance, the radical mechanism can be in principle associated to the **5m$_S$**→**5m$_T$** intersystem crossing, which promotes one electron from the $\pi_\perp$*n.b.* lone pair to the higher $\pi_\parallel^*$*a.b.* level (see Scheme 4). This process requires the not small energy cost of ~+16 kcal mol^{-1}, which remains almost constant for various imido ligands. It was reported the diradical triplet promotes the C–H homolysis of an allylic substrate, while a subsequent *rebound* mechanism restores the diamagnetism of the system.[29]

In the present case, the diradical mechanism can be safely excluded for any missing evidence of homolysis and the mentioned inactivity of TEMPO radical scavenger, when added to the reaction mixture (see above). It must be anticipated that the observed indole formation, first analyzed over the singlet Potential Energy Surface (PES), requires at some point an access to the triplet state for stereochemical and electronic reasons to be later illustrated.

Structural aspects of the imido-alkyne coupling. It is debated in literature whether an alkyne can be prone to either a nucleophile or an electrophilic attack.[30] In principle, the former mode is difficult for the unavailability of suitable vacant C p_π orbitals, which appear only in the high lying C≡C π* levels. These may be affected only by a rather strong base, which may otherwise favor the PhC≡CH deprotonation. In contrast, both the NR ligands of **5m$_S$** are weak donors with a more pronounced effect at the NAr ligand for the presence of the two electron withdrawing CF_3 aromatic substituents.

Examples of the coupling between an imido ligand with an alkyne were reported for early Transition Metal (TM) complexes,[31] while corresponding reactions involving late TM systems have been less investigated. The computationally ascertained energy profile of Scheme 5 starts from the separated species [Ru](NMe)(NAr) (**5m$_S$**) and phenylacetylene (**2a**), which jointly represent the initial zero energy point.

The optimized structure of the weak adduct **6m$_S$**, as the first encountered minimum, is shown at the top left side of Figure 6.[32] At its right side, the transition state **7m$_{S\text{-}TS}$** was first located *via* a relaxed scan technique that progressively shortened $N_1 \cdots C_1$ separation from 3.88 Å to the bonding value.

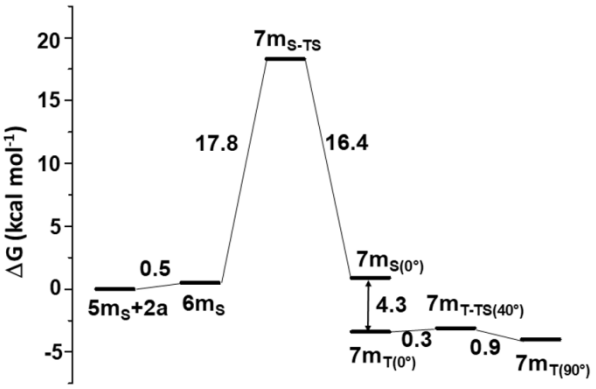

Scheme 5. Energy profile for the $\mathbf{5m_S}$+**2a** coupling, characterized by an intersystem crossing and the 90° rotation of the new amido ligand ($\mathbf{7m_{T(0°)}}$→$\mathbf{7m_{T(90°)}}$ transformation).

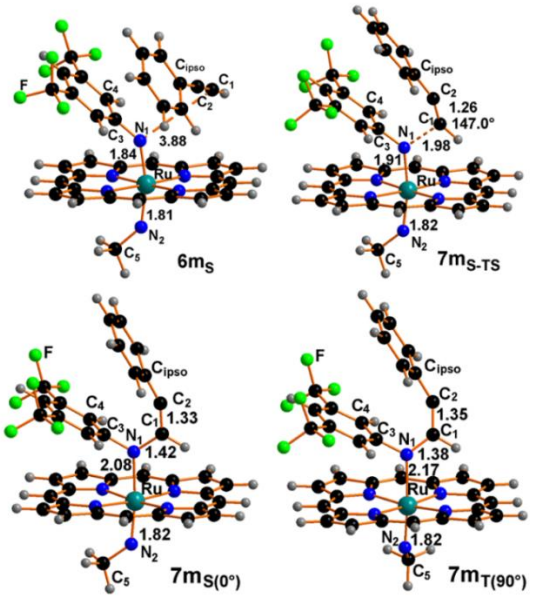

Figure 6. The $\mathbf{6m_S}$ adduct and the transition state $\mathbf{7m_{S\text{-}TS}}$ upon $N_1\cdots C_1$ coupling; the subsequent singlet complex $\mathbf{7m_{S(0°)}}$ and its triplet isomer $\mathbf{7m_{T(90°)}}$ with orthogonal imido/amido ligands.

The unique imaginary frequency at -383.5 cm^{-1} of the fully optimized species $\mathbf{7m_{S\text{-}TS}}$ is indicative of the N_1-C_1 stretching with the assignment further corroborated by an IRC analysis.

Although in $\mathbf{7m_{S\text{-}TS}}$ the N_1-C_1 separation is still as large as 1.98 Å,[33] the lost linearity of the alkyne moiety (H_1-C_1-C_2 and C_1-C_2-C_{ipso} angles of 147.0° and 157.0°, respectively) implies an electron density transfer from the N_1 atom into a $\pi_{\|}$* level. The latter point is also confirmed by the 0.04 Å elongation of the original $C_1{\equiv}C_2$ triple bond consistently with the computed 90 cm^{-1} red shift of the stretching frequency.

The total energy barrier of +18.3 kcal mol^{-1} to reach $\mathbf{7m_{T\text{-}TS}}$ may be indicatively compared with the +22.9 kcal mol^{-1} value found for the coupling of a 3-hexyne with the apical nitride ligand of a related ruthenium salen complex.[34] For comparison, an analogous path over the triplet PES is unlikely in view of the ~+20.0 kcal mol^{-1} higher barrier of $\mathbf{7m_{T\text{-}TS}}$ in Figure S19. The final singlet point $\mathbf{7m_{S(0°)}}$ (Figure 6) is characterized by a $C_5N_2N_1C_3$ dihedral angle of 0° that implies the co-planarity of the *trans* imido and amido axial ligands. The -16.4 kcal mol^{-1} energy gain in $\mathbf{7m_{S(0°)}}$ *vs*. $\mathbf{7m_{S\text{-}TS}}$ is mainly due to the exergonicity of the newly formed N_1-C_1 σ bond of 1.42 Å, which does not exclude some π delocalization over the adjacent $C_1{=}C_2$ linkage of 1.33 Å.[35] The singlet minimum $\mathbf{7m_{S(0°)}}$ also exists as the 4.3 kcal mol^{-1} more stable triplet isomer $\mathbf{7m_{T(0°)}}$ in Figure S20, which minimally differs for conformation and geometry. Under these circumstances, no reaction coordinate was identified for detecting the intersystem crossing barrier. However, $\mathbf{7m_{T(0°)}}$ further converts into the another triplet isomer, namely $\mathbf{7m_{T(90°)}}$ in Figure 6, which lies lower by only -0.6 kcal mol^{-1}. This occurs with an evident structural rearrangement with the 90° rotation of the *trans*-axial amido and imido ligands. About halfway (~40°), the Transition State $\mathbf{7m_{T\text{-}TS(40°)}}$ was identified (see Figure S21) with the flat energy barrier of +0.3 kcal mol^{-1}. The dangling chain Ru-N_1-C_1(H)=C_2Ph in all the structures of Figure 6 is indicative of a terminal vinyldenic anion, likely formed upon the *in plane* lone pair transfer from the N_1 atom to the terminal C_2 one. Similar features were previously detected by some of us (C.M. and G.M) in an experimental/theoretical study of an alkyne rearrangement over a Co-Co linkage.[36] Another similar example of a vinylidenic dangling chain has been proposed for a catalytic metallo-nitrene alkyne metathesis.[37] In any case, the terminal Ph substituent leans toward the aryl moiety at the N atom with potential steric problems for the five-membered ring closure (C_2-C_4 linkage, Figure 6). More importantly, the C_2 sp^2 conformation appears inadequate for the coupling due to the improper orientation of the C_2 σ hybrid. The orbital/electronic underpinnings of the imido-alkyne coupling are described in the following section.

Orbital/electron rearrangements in the imido-alkyne coupling preceding the ring closure. Figure 7 shows the ensemble of the three $1\pi_{\|}$, $2\pi_{\|}$ and $1\pi_{\perp}$ frontier MOs, which in both $\mathbf{7m_{S(0°)}}$ and $\mathbf{7m_{T(0°)}}$ have maximum width of ~0.80 eV. The two electrons available to the levels in question are consistent with both the singlet and the triplet state and, since the latter is more stable by only -4.3 kcal mol^{-1}, intersystem crossing cannot to be excluded.

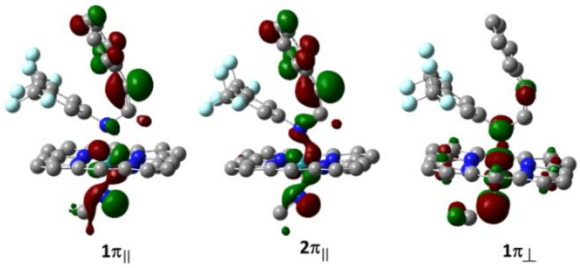

Figure 7. The close frontier levels of $\mathbf{7m_{S(0°)}}$ and $\mathbf{7m_{T(0)}}$, where $1\pi_{\|}$ and $2\pi_{\|}$ are either the HOMO and LUMO or the two SOMOs, respectively. In the triplet, $1\pi_{\perp}$ may also compete for electrons.

In the **7m$_{S(0°)}$**, 1$\pi_{||}$ and 2$\pi_{||}$ correspond to the HOMO and LUMO of the system with an energy gap of +0.40 eV, while in triplet **7m$_{T(0°)}$**, the same levels are the most probable SOMOs, which are separated by only 0.23 eV. On the other hand, also the slightly higher 1$\pi_{\perp}$ level may compete for population. To analyze the latter aspects, a more sophisticated treatment, such as one of the various multireference methods or the broken symmetry approach, would be more appropriate. However, due to the complexity of the system, we limited the investigation to the basic DFT method in association with perturbation theory arguments,[38] which were extracted from the simplified interaction and Walsh diagrams of Scheme 6.[39] Here, the left side diagram for **7m$_{S(0°)}$** highlights the three orbital interactions of the alkyne $\pi_{||}$ and $\pi_{||}$* combinations with either the $\pi_{||}$*n.b.* and $\pi_{||}$*a.b.* level (shown in Scheme 4) giving rise to the 1$\pi_{||}$ and 2$\pi_{||}$ MO, respectively.

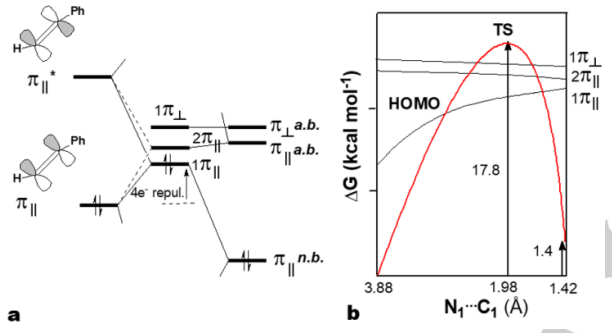

Scheme 6. a) General interaction diagram applicable to the singlet an triplet models of type **7m**. **b)** Evolution of the frontier levels in the **6m$_S$→7m$_{S(0°)}$** transformation (total energy in red).

Essentially, the two populated $\pi_{||}$ and $\pi_{||}$*n.b.* levels cause a significant 4e$^-$ repulsion, mitigated by the mixing of $\pi_{||}$* into 1$\pi_{||}$. This cancels out the *in-plane* C_1 p_π orbital from 1$\pi_{||}$ but enhances the C_2 one (first drawing of Figure 7). A similar $\pi_{||}$* mixing occurs in the antibonding $\pi_{||}$/$\pi_{||}$*a.b.* combination (a *2c/2e*$^-$ interaction), enhancing the weight of C_2 p_π in 2$\pi_{||}$, also shown in Figure 7. Conversely, 1$\pi_{\perp}$ maintains the original $\pi_{\perp}$*a.b.* character of Scheme 4 due to its symmetry properties.

The Walsh diagram, which monitors the frontier MOs upon the N_1···C_1 coupling, shows how the 4e$^-$ repulsion destabilizes 1$\pi_{||}$ up to the region of the vacant levels 2$\pi_{||}$ and 1$\pi_{\perp}$, with a reduced steepness of the curve after the TS. Then, the system stabilizes (red curve) thanks to the N_1-C_1 σ bond formation. At the **7m$_{S(0°)}$** minimum, 1$\pi_{||}$ becomes a C_2 lone pair of a vinylidene carbanion (Figure 8), similarly to another case already investigated by some of us.[40] This corresponds to the transfer of the *in plane* lone pair at the dianionic imido ligand of **5m$_S$** (box of Scheme 4) to the C_2 atom, hence the separation of the negative charges in **7m$_{S(0°)}$**, as shown in Figure 8.

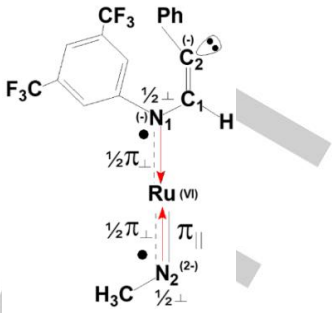

Figure 8. Structural formula of **7m$_{S(0°)}$** with separated charges at the N_1 and C_2 atoms.

The two electrons, which previously allowed two consecutive *in plane* Ru-N π half bonds, are now localized below the porphine macrocycle ensuring the MeN_2=Ru π linkage (solid line). Conversely, the $\pi_{\perp}$ distribution is substantially unaffected with respect to **5m$_S$**. In this manner, 6 and 7 electrons are counted for the N_1 (amido) and N_2 (imido) atoms, respectively, with the metal remaining Ru(VI).

The eventual closeness of the 1$\pi_{||}$, 2$\pi_{||}$ and 1$\pi_{\perp}$ levels allows a spontaneous formation of the triplet isomer **7m$_{T(0°)}$**, which promptly interconverts into **7m$_{T(90°)}$** (Scheme 5), where the 0.8 eV width of the three frontier MOs is maintained. The achieved orthogonality of the imido and amido ligands is a cornerstone of the process, as it will be clarified later. This implies a reshuffling of the $\pi_{||}$/$\pi_{\perp}$ combinations, as highlighted from the comparison of Figures 7 and 9. The latter shows that the C_2 sp^2 σ hybrid is now localized at the lowest of the three levels (1$\pi_{||}$), while 1$\pi_{\perp}$ lies higher by +0.5 eV. The highest 2$\pi_{||}$ and the lower 1$\pi_{\perp}$ MOs feature MeN_2=Ru d_π/p_π antibonding character.

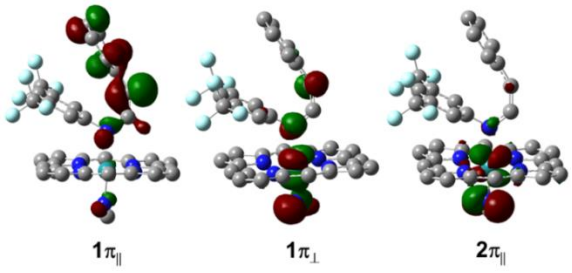

Figure 9. The three modified frontier MOs of **7m$_{T(90°)}$** as determined by the orthogonality of the amido and imido ligands.

In the staggered conformation of the *trans*-axial ligands of **7m$_{T(90°)}$**, the plane of the d_{xz} and d_{yz} orbitals also contains one of the N_{equat}-Ru-N_{equat} vectors, thus suggesting an involvement of the porphine's π system in the overall π electron delocalization. The result is confirmed by the computed spin densities of 0.28, 0.22 and 0.23 e^2 bohr^{-3} for the Ru, N_1 and N_2 atoms, respectively, plus a residual 0.25 e^2 bohr^{-3} value for the non-innocent porphine.

Structural and electronic aspects of the five-membered ring closure. In all the species examined up to now (see Figure 6), the C_2 sp^2 conformation is unsuited for a direct $C_2\cdots C_4$ coupling, hence the Ph alkyne's substituent must rotate by ~180° about the C_2=C_1 double bond. However, all of our attempts of validating either a singlet or a triplet intermediate of this type failed, since the corresponding model immediately converged to either the ring-closed isomer **8m$_S$** or **8m$_T$**; the former is shown in Figure 10. None of the latter species has ever been experimentally detected, but the *in silico* result indicates how the reaction proceeds through a complex of the closed bicyclic molecule **3aa$_{iso}$**, *i.e.,* an isomer of the final indole product **3aa**. At variance with the latter, **3aa$_{iso}$** is not planar due to the C_4 sp^3 hybridization and the still present C_4-H_4 bond. The lack of experimental evidence for any species of type **8** suggests that **3aa$_{iso}$** promptly separates from the metal and undergoes a subsequent *outer sphere* isomerization with the H_4 atom transfer from C_4 to N_1, as described in a following section.

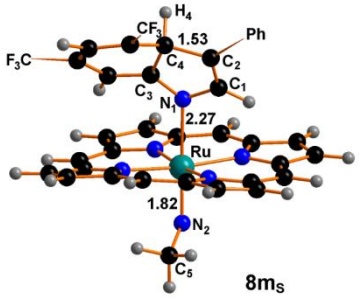

Figure 10. The optimized spin isomer **8m$_S$** that already features a 6+5 bicyclic molecule.

The *in silico* detection of both **8m$_S$** and **8m$_T$** (Figure S22) shows a weaker Ru-N_1 bonding in the former (2.27 *vs*. 2.20 Å) as well as a pronounced tilt of the coordinated five membered ring with respect to the octahedron's main axis (~30° *vs*. 8°). Thus, the loss of the bicyclic molecule more likely occurs at the singlet complex, which is also energetically favored by -4.8 kcal mol^{-1}. In this case, another intersystem crossing must occur after that of the **7m$_{S(0°)}$**→**7m$_{T(0°)}$** transformation. This is confirmed by the plot in Figure 11, which, by using a scan technique, monitors the shortening of the $C_2\cdots C_4$ distance and indicates the Minimum Energy Crossing Point (MECP).[41] Both the species **7m$_{S(0°)}$** and **7m$_{T(0°)}$** were fixed as starting points of the singlet (black) and triplet (red) curves, respectively. Perhaps, the constantly small energy difference seems to confirm the competitiveness of the two spin states in the process. The torsion about the C_1=C_2 linkage eventually reaches the values of 176° and 171° in **8m$_S$** and **8m$_T$**, respectively. The crossing point (CP) occurs at the $C_2\cdots C_4$ distance of ~2.37 Å with a torsion of ~145°. Then, the singlet species immediately stabilizes, while the triplet inverts its trend only at ~2.20 Å and never returns to be the lower isomer. Based on these data, the MECP is estimated to be as low as +3.4 kcal mol^{-1}.

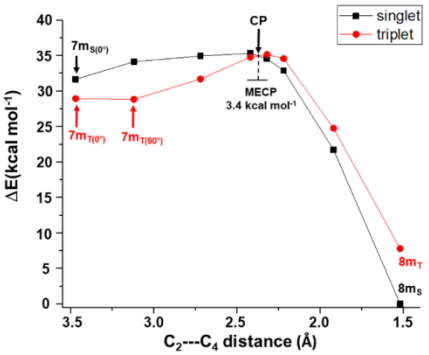

Figure 11. Singlet/triplet relaxed energy scans for the C_2-C_4 coupling, which associates to the torsion about the C_1=C_2 linkage.

To explain the orbital/electronic trends of Figure 11 it must be recalled that the minimum **7m$_{T(90°)}$** (Scheme 5) has the unpaired electrons in the orthogonal MOs of Figure 9, namely $1\pi_{\|}$ and $1\pi_{\perp}$. The single population of the latter suggests an allylic-type radical in the N_1=C_1=C_2 region, that presumably favors the rotation of the phenyl group and stereochemical inversion of the C_2 sp^2 center. Near the CP crossing point, the reorienting C_2 σ hybrid in $1\pi_{\|}$ starts "feeling" the C_4 one, which derives from a π bonding MO of the aryl ring. The level in question transforms into a C_4 sp^3 lone pair thanks to the pinning down of the C_4-H_4 linkage, as indicated by the structure in Figure 10. The resulting C_2-C_4 σ* combination (Figure 12) is swept away from the frontier region, leaving only the two orthogonal and close MeN_2=Ru π* combinations of Figure 9. Hence, the two available electrons are either paired or unpaired at the levels $1\pi_{\perp}$ and $2\pi_{\|}$, even if the singlet **8m$_S$** is somewhat favored after the CP. The feature persists even after the separation of the [Ru](NMe) (**Am$_S$**) fragment from the bicyclic molecule, already suggesting that the spin multiplicity is intrinsic in the metal fragment (**Am$_S$** is -5.0 kcal mol^{-1} more stable than **Am$_T$**).

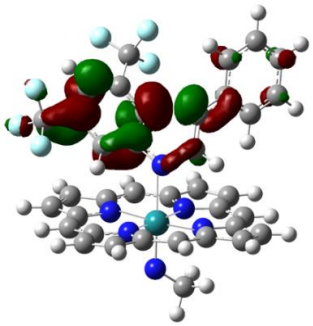

Figure 12. The C_4-C_2 σ* destabilizing level upon the ring closure in either **8m$_S$** or **8m$_T$**.

The formation of the C_2-C_4 σ bond is consistent with a typical chemical substitution at the aromatic ring of the original ArN imido grouping. In principle, the process may have alternative

nucleophilic or electrophilic character, depending on the inductive and/or π delocalization effects of the aryl substituents, which determine a different regioselectivity.[42] In the case of the present aryl ring with EWG substituents at *para* and *ortho* positions with respect to the C_4 atom plus the *ortho* amido EDG one, the evolution of the process is hardly predictable, even if some MO consideration support the electrophilic substitution. While the C_2 vinylidenic anion proposed for the singlet **7m$_{S(0°)}$** of Figure 8 would suggest a nucleophilic attack, the picture is significantly modified at the triplet **7m$_{T(90°)}$**. In fact, the half vacated $1\pi_{\|}$ level already implies a partial electrophilicity of the C_2 atom that could be already attacked by the C_4 sp^3 lone pair to give the **3aa$_{iso}$** bicyclic molecule in **8m$_T$**. The effect is definitely magnified when $1\pi_{\|}$ is totally vacated in the singlet ground state. The scission of **3aa$_{iso}$** from either **8m$_S$** or **8m$_T$** is similarly endergonic (+10.1 and +12.3 kcal mol^{-1}, respectively), mainly due to the active dispersion forces, in spite of the weak Ru-N_1 σ linkage of 2.27 in the singlet complex. It may be discharged that **3aa$_{iso}$** may separate as a triplet for its +28 kcal mol^{-1} higher energy, that excludes the final indole formation to be radical. It remains to establish whether the process of the **3aa$_{iso}$ →3aa** isomerization already starts when the bicycle is still anchored to the metal or is an *outer sphere* process. The latter point will be described in more details in a separate section.

Electronic/orbital aspects of the [Ru](NMe) (Am) catalyst. Upon the departure of the formed bicyclic molecule, the residual five-coordinated metal fragment is either the singlet **Am$_S$** or the triplet **Am$_T$**. In any case, there remain six π electrons, which differently affect the nature of the MeN_2=Ru multiple bonding. As qualitatively shown in Scheme 7a, there are 2+2 orthogonal bonding and antibonding levels with one electron pair being available to the two π* combinations. Depending on the $\pi_{\|}^*$-$\pi_{\perp}^*$ gap, the two electrons may be either coupled or split, determining the **Am$_S$** or the **Am$_T$** spin isomers, respectively.

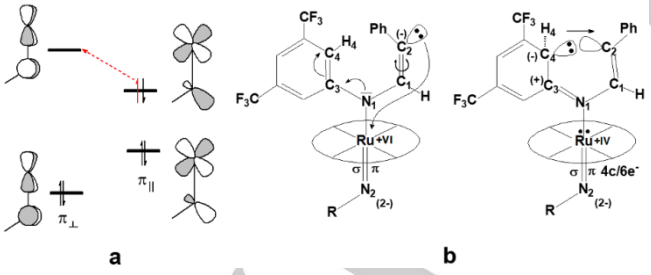

Scheme 7. a) π electron distribution in the **Am**–type compounds. b) Evolution of the highest π* electron pair for **Am** along the pathway leading first to **8m$_S$** or **8m$_T$**.

A consistent picture also applies to the immediate precursors **8m$_S$** or **8m$_T$**. In any case, an overall MeN=Ru double bond exists, since the two highest electrons either allow a full double bond (vacant $\pi_{\perp}$*) or two half π bonds (two SOMOs). The two available π* electrons are those of the filled C_2 σ hybrid at the intermediate **7m$_{S(0°)}$**, which were in turn derived from one pristine alkyne C≡C π linkage. Remarkably, the described electron redistribution implies an inner Ru(VI)→Ru(IV) reduction with respect to the starting *bis*-imido complex (**5m$_S$**). The mentioned electron relationships are illustrated in Scheme 7b, that shows how one imido dianion first transforms into an amido and then into an uncharged imino ligand upon the C_2-C_4 coupling.

Aspects of the isomerization of the 3aa$_{iso}$ bicyclic molecule to the indole 3aa. The process most likely occurs on the singlet PES involving the C_4→C_3→N_1 stepwise transfer of the H_4 atom throughout the bicyclic molecule. It remains to establish at which point the latter detaches from the metal. Recall that in the starting **8m$_S$** complex (Figure 10) the large Ru-N_1 distance of 2.27 Å and the 29° bias of the five-membered ring already suggested a poor coordination in spite of the +10.1 kcal mol^{-1} cost for the scission, which is contrasted by the dispersion forces. To frame better the picture, we first examined the *outer sphere* isomerization, as shown in Scheme 8.

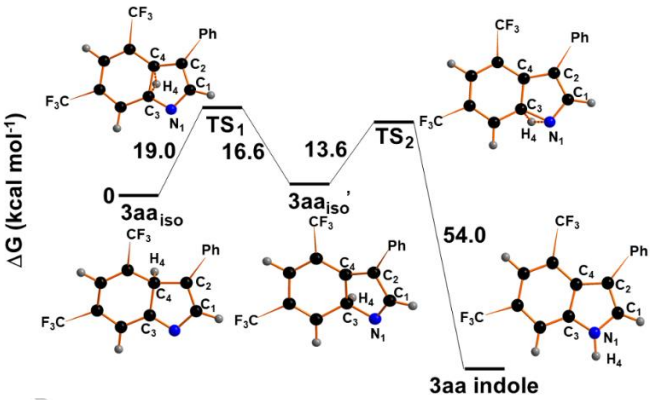

Scheme 8. Free energy profile for the *outer sphere* **3aa$_{iso}$→3aa** isomerization.

The first intermediate **3aa$_{iso}$'** is attained through the TS_1 barrier of +19.0 kcal mol^{-1} due to disfavoring H_4 bridging position in between the C_4 and C_3 atoms.[43] Not all of the lost energy is recovered at **3aa$_{iso}$'**, which lies +2.4 kcal mol^{-1} above **3aa$_{iso}$**, while the major energy gain occurs at the subsequent step. Here, the N_1 imino lone pair, which was originally engaged in metal coordination, is used for the final N_1-H_4 linkage. The encountered TS_2 barrier of +13.6 kcal mol^{-1} is again attributable to the H_4 bridging position in between the C_3 and N_1 atoms. After TS_2, the system gains as much as -54.0 kcal mol^{-1} thanks to the achieved planarity and aromaticity of the indole. Overall, the *outer sphere* process of Scheme 8 is as exergonic as -37.9 kcal mol^{-1}.

Alternatively, we also considered that the isomerization of **3aa$_{iso}$** starts while the bicyclic molecule still anchored to the metal. In fact, by excluding the dissociation of **8m$_S$**, the intermediate complex **9m** could be fully optimized as shown in Figure S23. In the latter, the **3aa$_{iso}$'** isomer acts as a donor to the metal by still using the N_1 lone pair without any major penalization of the Ru-N_1 strength nor the stereochemistry of the bicyclic molecule. This is corroborated by the very similar binding energies of **8m$_S$** and **9m**, with the latter being disfavored by only +1.3 kcal mol^{-1}.

Implicitly, **9m** must dissociate to free the N_1 lone pair for allowing the **3aa** formation. In this respect, it must be mentioned that the scission of **9m** is more expensive than that of **8m$_S$** (+13 *vs*. +10.1 kcal mol^{-1}). From this data, it is hard to predict which of the two alternative pathways of the isomerization is more likely.

Influence of the electronic characteristics of aryl azide on the catalytic mechanism. Amongst our experiments, the formation of indole was investigated for the reaction between PhC≡CH and selected azides of formula 3,5-$X_2C_6H_3N_3$ (X = CF_3, Cl and Me). Even if the most efficient process occurs when X = CF_3, the catalysis also proceeds if X = Cl with the formation of the corresponding indole with 60% yield (*vs*. 86% yield observed when X = CF_3) (see Table 1). Conversely, for X = Me the reaction did not occur at all. To shed some light on the different behaviors, the already illustrated reactivity pathways were computationally tested also for azides bearing the Cl and Me EDG substituents besides the CF_3 EWG ones. In any case, the calculations indicated quite similar trends and no evidence emerged that the EDG groups significantly alter the features of the five-membered ring closure. In view of the similar computed mechanistic behaviors for differently substituted azides, we looked for some alternative explanation of the experimental reactivity. With reference to the *path a* of Scheme 3, we focused on the formation of the *bis*-imido species **C** from the five-coordinated fragment **Am** and variously substituted azides. As previously shown,[17] the azide must first anchor to the metal to be activated over the singlet PES *via* the N_2 loss. In Scheme 9, the free energy profiles of the species with Me, Cl and CF_3 substituents outline a potential exergonic access to the *bis*-imido complex **C** (or **5m$_S$** in the case of X = CF_3). To shed some light on the missed **C** formation in the case of X = Me, one must focus on the stability of the initial adduct **B** and the relative difficulty in attaining the subsequent **TS**.

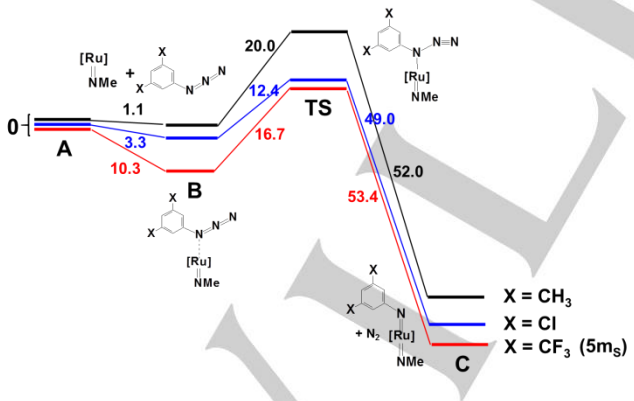

Scheme 9. Comparative energy underpinnings of the *bis*-imido complex **C** formation, which is inhibited in presence of methyl EDG aromatic substituents.

By assuming constant dispersion and entropy terms, the estimated energy order of the **B** compounds (namely -10.3, -3.3 and -1.1 kcal mol^{-1} for X = CF_3, Cl and Me, respectively) is mainly due to the enthalpy effects introduced by the different substituents. The Me-containing species has not only the least favoured starting point **B** but also features the highest **TS** barrier of +20.0 kcal mol^{-1} possibly in line with its chemical inertness. On the other hand, the profiles of the Cl and CF_3 substituted compounds may be consistent with their reactivity in producing corresponding indoles with different yields (Table 1). The adduct **B** has the largest stability in the CF_3 case, implying a sufficient lifetime to continue the reaction. From this viewpoint, the +7.0 kcal mol^{-1} higher energy of the **B** chlorine analogue seems to disfavour the process, which is however not inhibited because of the rather low TS barrier to be passed.

The exergonicity of all the reactions in Scheme 9 may seem inconsistent with the lack of the reactivity for the X = Me. Some weak points in the profile of the latter species have already been illustrated and it cannot be excluded that the initially disfavouring thermal effects may influence the kinetic behaviours.

Conclusions

The Ru(TPP)$(NAr)_2$ (**5**) complex showed a very good catalytic activity in promoting the synthesis of C_3-substituted indoles (up to 30 examples) by the one-pot reaction of aryl azides with alkynes. The study of the reaction scope revealed that the reaction is very efficient and completely regioselective for terminal alkynes and aryl azides bearing on the 3 and 5 aromatic positions the same electron withdrawing group. It should be noted that when the 3,5-$(NO_2)_2C_6H_3N_3$ azide was reacted with different alkynes, the corresponding indoles precipitated from the reaction mixture in a pure form. Thus, a convenient filtration, instead of less sustainable and more expensive purification procedures (e.g. chromatographic purification), was used to isolate the desired compounds.

The joint experimental/theoretical study rationalized the catalytic indole formation with the key mechanistic aspects being supported by orbital and electronic arguments. In particular, it emerged how the stereochemistry of the system is dynamically affected by an interplay of singlet and triplet ground states that eventually allows the conformational inversion of the sp^2 C (Ph) atom. Also, thanks to the vacancy of the latter an electrophilic attack to one aryl's position allows the C-C coupling. Then, the formed bicyclic molecular skeleton detaches from the metal with a subsequent *outer sphere* isomerization affording the desired indole. At this point, the separated five-coordinated *mono*-imido species **A** (Scheme 3) represents the actual reaction catalyst that repetitively activates a new azide molecule.[23c] The role of the EWG *vs*. the EDG substituents at the aryl ring of the azide has been compared to explain the correlation between the catalytic performance and the stability and lifetime of the initial ruthenium/azide adduct complex (**B** type). For convenience, Scheme 10 summarizes the overall mechanism with the stepwise energies. A more standard reaction profile is presented in Scheme S1 (SI).

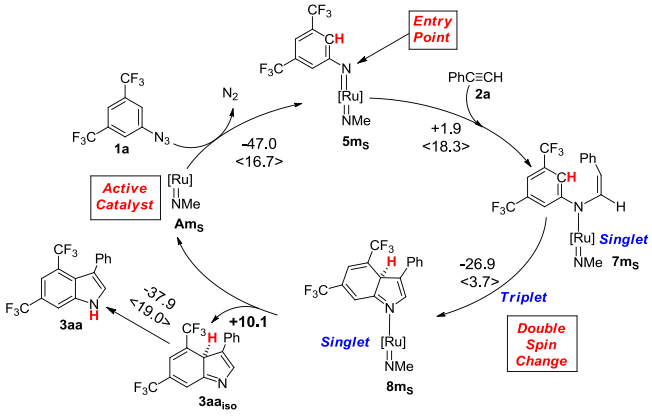

Scheme 10. Suggested catalytic cycle of the azide/alkyne coupling leading to indole. ΔG values (kcal mol^{-1}) are reported for each step together with the associated barrier (in brackets).

The process starts with the reaction of *bis*-imido complex **5m$_S$** with an alkyne to give the singlet intermediate **7m$_S$** featuring a dangling chain. The terminal C(Ph) atom of **7m$_S$** has an unsuited sp^2 conformation for the coupling with the aryl ring, hence the system undergoes a stereochemical rearrangement. This is allowed by a double intersystem crossing (singlet→triplet→singlet), whose implications for the mechanism were underlined. In this manner, the bicyclic skeleton **3aa$_{iso}$** is formed as a ligand in **8m$_S$** through an aromatic-like electrophilic substitution. Notice that such a step implies an inner redox process, namely Ru(VI)→Ru(IV) reduction and amido→imino oxidation (see Scheme 7b). Finally, the **3aa$_{iso}$** bicyclic molecule dissociates from the metal and undergoes two subsequent H migration steps to give the final indole **3aa**. Importantly, the separation of the bicyclic molecule affords the five-coordinated metal fragment [Ru](NMe) (**Am**) as the active catalyst, which activates a new azide molecule and restores the *bis*-imido precursor **5m**. Overall, the indole formation is energetically highly favored (*i.e.,* -99.9 kcal mol^{-1}) with the largest barrier of +19.0 kcal mol^{-1}. Notice that the latter is found for the indole outer sphere isomerization, while in the metal-catalyzed cycle, a very similar barrier of +18.3 kcal mol^{-1} was estimated to reach **7m$_{S\text{-}TS}$** (Scheme 5). Based on the energy closeness, no precise information arises about the actual rate determining step, for which not even the kinetics offers useful indications.

Experimental Section

Computational Details. . All of the models were optimized at the B97D-DFT level of theory[44] by using the Gaussian 09 package.[45] Minima and/or transition states were validated by vibrational frequencies. The CPCM model[46] was used to mimic the experimentally used benzene solvent. The effective Stuttgart/Dresden core potential (SDD)[47] was adopted for ruthenium with the 6-31G+(d, p) basis set for all the other atoms.[48] To confirm the acceptability of the latter original approach, several optimizations were also carried out with the triple zeta basis set def2-TZVP.[49] The structural and energy divergences appear minor as it can be verified in the Supporting Information, which besides all the optimized species, includes pairwise sets of coordinates, when available. Also, the coordinates of some key models such as **5m$_S$'**, **5m$_T$'**, **7m$_S$'**, **7m$_T$'**, **8m$_S$'** and **8m$_T$'**, with 3,5-(CF$_3$)$_2$C$_6$H$_3$ substituents at both the *N*-imido groups, are given in the SI to support the consistency with the used simpler models. Qualitative MO arguments were developed with the CACAO package[39] after verifying the gross consistency between EHMO and DFT results.

General. All reactions were carried out under nitrogen atmosphere employing standard Schlenk techniques and vacuum-line manipulations. Anhydrous benzene was purified by using standard procedures and stored under inert atmosphere. Organic azides[50] and Ru(TPP)(NAr)$_2$ (**5**)[19b] were synthesized by methods reported in literature. Phenylacetylene (**2a**) was filtered over activated alumina, distilled and stored under nitrogen. All the other starting materials were commercial products and used as received. NMR spectra were recorded at room temperature either on Bruker Avance 300-DRX, operating at 300 MHz for ^{1}H, at 75 MHz for ^{13}C and at 282 MHz for ^{19}F, or on a Bruker Avance 400-DRX spectrometers, operating at 400 MHz for ^{1}H NMR, 100 MHz for ^{13}C and 376 MHz for ^{19}F. Chemical shifts (ppm) are reported relative to TMS. The ^{1}H NMR signals of the compounds described in the following have been attributed by COSY and NOESY techniques. Assignments of the resonance in ^{13}C NMR were made by using the APT pulse sequence and HSQC and HMBC techniques. GC-MS analyses were performed on a Shimadzu QP5050A equipped with Supelco SLB -5 ms capillary column (L 30m × I.D. 0.25 µm film thickness). GC analyses were performed on a Shimadzu GC-2010 equipped with a Supelco SLB -5 ms capillary column (L 10m × I.D. 0.1 µm film thickness). Infrared spectra were recorded on a Varian Scimitar FTS 1000 spectrophotometer. UV-Vis spectra were recorded on an Agilent 8453 instrument. Mass spectra were recorded in the analytical laboratories of Milan University. Microanalyses were performed on a Perkin Elmer 2400 CHN Elemental Analyzer instrument.

Procedure for catalytic reactions. Method A: Alkyne (2.5 mmol) and aryl azide (0.50 mmol) were added to a benzene (10 mL) solution of complex **5** (11.7 mg, 0.010 mmol) and the resulting mixture was refluxed until the complete conversion of aryl azide, which was monitored by IR spectroscopy ($\nu_{N=N}$ = 2200-2000 cm^{-1}). The solvent was evaporated to dryness and the crude purified by flash chromatography. **Method B:** the procedure was identical to that described in method A except for the purification step. After the complete conversion of aryl azide, desired products were collected in a filter in a pure form. **Method C:** the procedure was identical to that described in method A, except for the amount (1.1 mL, 10.0 mmol) of employed phenylacetylene (**2a**). At the end of the reaction, the **2a** excess was recovered in 90-95% yield (GC analysis, biphenyl as the internal standard) by vacuum distillation of the obtained mixture.

Synthesis of indole 3aa from Ru(TPP)(NAr)$_2$ (5) and phenylacetylene (2a). Phenylacetylene (**2a**) (27 µL, 0.24 mmol) was added to a benzene (30.0 mL) solution of complex **5** (57.4 mg, 0.049 mmol) and the resulting solution was refluxed until the complete disappearance of **5** (TLC monitoring, Al_2O_3, *n*-hexane/CH_2Cl_2 = 9:1). GC-MS analysis revealed the formation of compound **3aa** that was isolated by flash chromatography (SiO_2, *n*-hexane/AcOEt = 9:1) (50% yield, considering the transfer of only one nitrene functionality from **5** to **2a**).

Isotope tracing experiment using phenylacetylene-*d*$_1$ (2a-*d*$_1$). Compound **1a** (86 µL, 0.50 mmol) and **2a-*d*$_1$** (99 atom % D) (275 µL, 2.5 mmol) were added to benzene (10.0 mL) solution of complex **5** (11.7 mg, 0.010 mmol). The resulting mixture was refluxed for 1.0 h until the complete aryl azide conversion. ^{1}H NMR (400 MHz, $CDCl_3$) spectrum of

the purified indole showed the absence of the signal attributed to C_2-*H* atom of the indole ring (Figure S2).

Kinetic Isotope Effect (KIE) experiment. Compound **2a** (275 μL, 2.5 mmol) and an equimolar mixture of **1a** (43 μL, 0.25 mmol) and **1a-*d*$_3$** (94 atom % D) (for details see supporting information) (44 μL, 0.25 mmol) were added to a benzene (10.0 mL) solution of complex **5** (12.0 mg, 0.010 mmol). The solution was refluxed for 15 minutes until the azide conversion of 35% was reached. The solvent was evaporated to dryness and the crude was purified by flash chromatography (SiO_2, *n*-hexane/AcOEt = 9:1) to give a mixture of **3aa** and **3aa-*d*$_2$** (the labile D of the $N_{(indole)}$-D bond was replaced by H during the purification). The k_H/k_D ratio of 1.1 was determined by ^{1}H NMR spectroscopy (300 MHz, $CDCl_3$) (Figure S3).

Synthesis of 3aa in the presence of TEMPO. Compounds **1a** (86 μL, 0.50 mmol), **2a** (275 μL, 2.5 mmol) and TEMPO (21.0 mg, 0.13 mmol) were added to a benzene (10.0 mL) solution of complex **5** (11.7 mg, 0.010 mmol) and the resulting solution was refluxed for 1.3 h until the complete consumption of aryl azide **1a**. The solvent was evaporated to dryness and the crude purified by flash chromatography (SiO_2, *n*-hexane/AcOEt = 9:1) (125.0 mg of **3aa**, 76%).

General kinetic procedure. Compounds **2a** and **1a** were added to a benzene (5.0 mL) solution of complex **5** under nitrogen. The flask was capped with a rubber septum and immediately placed in an oil bath preheated to 75°C. The aryl azide consumption was followed by IR spectroscopy ($\nu \approx 2114$ cm^{-1}) by withdrawing samples of the solution (0.1 mL) at regular time intervals. The apparent first order rate constants were fitted to the equation $-d[ArN_3]/dt = k_{app}[\mathbf{5}][\mathbf{1a}][\mathbf{2a}]$. The catalyst concentration was calculated by the exact amount of catalyst weighed in each run and was considered to remain constant during the reaction. See SI for other experimental details.

Acknowledgements

We are grateful to prof. Fabio Ragaini of University of Milan for his valuable suggestions regarding the kinetic study.
G.M. and C.M. acknowledge the ISCRA-CINECA (HP grant HP10C2Q178 and HP10CFMSCC) for the computational resources.

Keywords: indole • azide • ruthenium • porphyrin • DFT • energy profiles

[1] a) S. Lancianesi, A. Palmieri, M. Petrini, *Chem. Rev.* **2014**, *114*, 7108-7149; b) L. C. Klein-Junior, C. d. Santos Passos, A. P. Moraes, V. G. Wakui, E. L. Konrath, A. Nurisso, P.-A. Carrupt, C. M. Alves de Oliveira, L. Kato, A. T. Henriques, *Curr. Top. Med. Chem.* **2014**, *14*, 1056-1075.

[2] a) N. Chadha, O. Silakari, *Eur. J. Med. Chem.* **2017**, *134*, 159-184; b) S. Thokchom Prasanta, S. Okram Mukherjee, *Mini-Rev. Med. Chem.* **2018**, *18*, 9-25; c) S. Suzen, *Curr. Org. Chem.* **2017**, *21*, 2068-2076; d) D. Goyal, A. Kaur, B. Goyal, *ChemMedChem* **2018**, *13*, 1275-1299.

[3] E. Fischer, H. Hutz, *Ber.* **1895**, *28*, 585-587.

[4] a) J. Yamaguchi, A. D. Yamaguchi, K. Itami, *Angew. Chem. Int. Ed.* **2012**, *51*, 8960-9009; b) G. R. Humphrey, J. T. Kuethe, *Chem. Rev.* **2006**, *106*, 2875-2911; c) K. Krüger, A. Tillack, M. Beller, *Adv. Synth. Catal.* **2008**, *350*, 2153-2167; d) M. Inman, C. J. Moody, *Chem. Sci.* **2013**, *4*, 29-41; e) G. W. Gribble, *J. Chem. Soc., Perkin Trans. 1* **2000**, 1045-1075; f) M. Bandini, *Org. Biomol. Chem.* **2013**, *11*, 5206-5212; g) S. Cacchi, G. Fabrizi, *Chem. Rev.* **2011**, *111*, PR215-PR283; h) M. G. Ciulla, S. Zimmermann, K. Kumar, *Org. Biomol. Chem.* **2019**, *17*, 413-431.

[5] a) J.-B. Chen, Y.-X. Jia, *Org. Biomol. Chem.* **2017**, *15*, 3550-3567; b) S. Cacchi, G. Fabrizi, *Chem. Rev.* **2005**, *105*, 2873-2920; c) Y. Yang, Z. Shi, *Chem. Commun.* **2018**, *54*, 1676-1685; d) Q. Q. Cheng, Y. Yu, J. Yedoyan, M. P. Doyle, *ChemCatChem* **2018**, *10*, 488-496; e) J. A. Leitch, Y. Bhonoah, C. G. Frost, *ACS Catal.* **2017**, *7*, 5618-5627; f) T. A. Shah, P. B. De, S. Pradhan, T. Punniyamurthy, *Chem. Commun.* **2019**, *55*, 572-587; g) J. Kalepu, P. Gandeepan, L. Ackermann, L. T. Pilarski, *Chem. Sci.* **2018**, *9*, 4203-4216.

[6] B. C. G. Soderberg, *Curr. Org. Chem.* **2000**, *4*, 727-764.

[7] S. W. Youn, T. Y. Ko, *Asian J. Org. Chem.* **2018**, *7*, 1467-1487.

[8] a) R. C. Larock, E. K. Yum, *J. Am. Chem. Soc.* **1991**, *113*, 6689-6690; b) D. F. Taber, P. K. Tirunahari, *Tetrahedron* **2011**, *67*, 7195-7210; c) L. Ackermann, L. T. Kaspar, C. J. Gschrei, *Chem. Commun.* **2004**, 2824-2825; d) J. Barluenga, M. A. Fernández, F. Aznar, C. Valdés, *Chem. Eur. J.* **2005**, *11*, 2276-2283; e) J. Barluenga, F. J. Fañanás, R. Sanz, Y. Fernández, *Chem. Eur. J.* **2002**, *8*, 2034-2046; f) X.-S. Ning, X. Liang, K.-F. Hu, C.-Z. Yao, J.-P. Qu, Y.-B. Kang, *Adv. Synth. Catal.* **2018**, *360*, 1590-1594.

[9] a) N. Yoshikai, Y. Wei, *Asian J. Org. Chem.* **2013**, *2*, 466-478; b) B. J. Stokes, T. G. Driver, *Eur. J. Org. Chem.* **2011**, 4071-4088; c) F. Collet, R. H. Dodd, P. Dauban, *Chem. Commun.* **2009**, 5061-5074.

[10] a) S. Würtz, S. Rakshit, J. J. Neumann, T. Dröge, F. Glorius, *Angew. Chem. Int. Ed.* **2008**, *47*, 7230-7233; b) X.-L. Lian, Z.-H. Ren, Y.-Y. Wang, Z.-H. Guan, *Org. Lett.* **2014**, *16*, 3360-3363; c) J. J. Neumann, S. Rakshit, T. Dröge, S. Würtz, F. Glorius, *Chem. Eur. J.* **2011**, *17*, 7298-7303; d) Z. He, W. Liu, Z. Li, *Chem. Asian J.* **2011**, *6*, 1340-1343; e) R. Bernini, G. Fabrizi, A. Sferrazza, S. Cacchi, *Angew. Chem. Int. Ed.* **2009**, *48*, 8078-8081; f) W.-Q. Liu, T. Lei, Z.-Q. Song, X.-L. Yang, C.-J. Wu, X. Jiang, B. Chen, C.-H. Tung, L.-Z. Wu, *Org. Lett.* **2017**, *19*, 3251-3254; g) X. Mao, T. Tong, S. Fan, L. Fang, J. Wu, X. Wang, H. Kang, X. Lv, *Chem. Commun.* **2017**, *53*, 4718-4721; h) S. Tang, X. Gao, A. Lei, *Chem. Commun.* **2017**, *53*, 3354-3356.

[11] a) Y. Wei, I. Deb, N. Yoshikai, *J. Am. Chem. Soc.* **2012**, *134*, 9098-9101; b) Z. Shi, F. Glorius, *Angew. Chem. Int. Ed.* **2012**, *51*, 9220-9222; c) P. S. Naidu, S. Kolita, M. Sharma, P. J. Bhuyan, *J. Org. Chem.* **2015**, *80*, 6381-6390.

[12] a) F. Ragaini, A. Rapetti, E. Visentin, M. Monzani, A. Caselli, S. Cenini, *J. Org. Chem.* **2006**, *71*, 3748-3753; b) F. Ragaini, F. Ventriglia, M. Hagar, S. Fantauzzi, S. Cenini, *Eur. J. Org. Chem.* **2009**, *2009*, 2185-2189; c) A. Penoni, K. M. Nicholas, *Chem. Commun.* **2002**, 484-485.

[13] a) B. Liu, C. Song, C. Sun, S. Zhou, J. Zhu, *J. Am. Chem. Soc.* **2013**, *135*, 16625-16631; b) C. Wang, Y. Huang, *Org. Lett.* **2013**, *15*, 5294-5297; c) A. Penoni, G. Palmisano, Y.-L. Zhao, K. N. Houk, J. Volkman, K. M. Nicholas, *J. Am. Chem. Soc.* **2008**, *131*, 653-661; d) F. Tibiletti, M. Simonetti, K. M. Nicholas, G. Palmisano, M. Parravicini, F. Imbesi, S. Tollari, A. Penoni, *Tetrahedron* **2010**, *66*, 1280-1288; e) S. Muthusamy, A. Balasubramani, E. Suresh, *Org. Biomol. Chem.* **2018**, *16*, 756-764; f) S. Muthusamy, A. Balasubramani, E. Suresh, *Adv. Synth. Catal.* **2017**, *359*, 786-790; g) G. Ieronimo, G. Palmisano, A. Maspero, A. Marzorati, L. Scapinello, N. Masciocchi, G. Cravotto, A. Barge, M. Simonetti, K. L. Ameta, K. M. Nicholas, A. Penoni, *Org. Biomol. Chem.* **2018**, *16*, 6853-6859.

[14] a) M. Peña-López, H. Neumann, M. Beller, *Chem. Eur. J.* **2014**, *20*, 1818-1824; b) Z. Shi, C. Zhang, S. Li, D. Pan, S. Ding, Y. Cui, N. Jiao, *Angew. Chem. Int. Ed.* **2009**, *48*, 4572-4576; c) L. Ackermann, A. V. Lygin, *Org. Lett.* **2012**, *14*, 764-767; d) Y. Liang, N. Jiao, *Angew. Chem. Int. Ed.* **2016**, *55*, 4035-4039; e) J. Wang, M. Wang, K. Chen, S. Zha, C. Song, J. Zhu, *Org. Lett.* **2016**, *18*, 1178-1181; f) J. Su, K. Zhang, M. Zhuang, F. Ma, W.-Q. Zhang, H. Sun, G. Zhang, Y. Jian, Z. Gao, *Asian J. Org. Chem.* **2019**, *8*, 482-486.

[15] a) M. P. Huestis, L. Chan, D. R. Stuart, K. Fagnou, *Angew. Chem. Int. Ed.* **2011**, *50*, 1338-1341; b) D. R. Stuart, P. Alsabeh, M. Kuhn, K.

Fagnou, *J. Am. Chem. Soc.* **2010**, *132*, 18326-18339; c) P. Patel, G. Borah, *Eur. J. Org. Chem.* **2017**, *2017*, 2272-2279.

[16] a) S. Cenini, F. Ragaini, E. Gallo, A. Caselli, *Curr. Org. Chem.* **2011**, *15*, 1578-1592; b) T. G. Driver, *Org. Biomol. Chem.* **2010**, *8*, 3831-3846; c) J. G. Harrison, O. Gutierrez, N. Jana, T. G. Driver, D. J. Tantillo, *J. Am. Chem. Soc.* **2016**, *138*, 487-490; d) N. Jana, T. G. Driver, *Org. Biomol. Chem.* **2015**, *13*, 9720-9741; e) C. Kong, N. Jana, C. Jones, T. G. Driver, *J. Am. Chem. Soc.* **2016**, *138*, 13271-13280; f) S. Parisien-Collette, C. Cruche, X. Abel-Snape, S. K. Collins, *Green Chem.* **2017**, *19*, 4798-4803; g) B. Lu, Y. Luo, L. Liu, L. Ye, Y. Wang, L. Zhang, *Angew. Chem. Int. Ed.* **2011**, *50*, 8358-8362; h) X.-R. Song, R. Li, T. Yang, J. Bai, R. Yang, X. Chen, H. Ding, Q. Xiao, Y.-M. Liang, *Tetrahedron Lett.* **2018**, *59*, 3763-3766.

[17] P. Zardi, A. Savoldelli, D. M. Carminati, A. Caselli, F. Ragaini, E. Gallo, *ACS Catal.* **2014**, *4*, 3820-3823.

[18] Z.-Y. Gu, J.-H. Li, S.-Y. Wang, S.-J. Ji, *Chem. Commun.* **2017**, *53*, 11173-11176.

[19] a) D. Intrieri, A. Caselli, F. Ragaini, P. Macchi, N. Casati, E. Gallo, *Eur. J. Inorg. Chem.* **2012**, 569-580; b) S. Fantauzzi, E. Gallo, A. Caselli, F. Ragaini, N. Casati, P. Macchi, S. Cenini, *Chem. Commun.* **2009**, 3952-3954.

[20] J. Wei, W. Xiao, C.-Y. Zhou, C.-M. Che, *Chem. Commun.* **2014**, *50*, 3373-3376.

[21] a) K. Banert, S. Bochmann, M. Hagedorn, F. Richter, *Tetrahedron Lett.* **2013**, *54*, 6185-6188; b) D. J. Anderson, T. L. Gilchrist, C. W. Rees, *Chem. Commun.* **1969**, 147; c) G. Dequirez, V. Pons, P. Dauban, *Angew. Chem. Int. Ed.* **2012**, *51*, 7384-7395.

[22] a) C. Wu, J. Li, B. Yan, *Dalton Trans.* **2014**, *43*, 5364-5374; b) D. F. Taber, W. Tian, *J. Am. Chem. Soc.* **2006**, *128*, 1058-1059; c) S. Jana, M. D. Clements, B. K. Sharp, N. Zheng, *Org. Lett.* **2010**, *12*, 3736-3739.

[23] a) P. Zardi, A. Pozzoli, F. Ferretti, G. Manca, C. Mealli, E. Gallo, *Dalton Trans.* **2015**, *44*, 10479-10489; b) G. Manca, C. Mealli, D. M. Carminati, D. Intrieri, E. Gallo, *Eur. J. Inorg. Chem.* **2015**, *2015*, 4885-4893; c) G. Manca, E. Gallo, D. Intrieri, C. Mealli, *ACS Catal.* **2014**, 823-832.

[24] T. A. Albright, J. K. Burdett and M.-H. Whangbo in *Orbital Interactions in Chemistry*, Second Edition, 2013, 834 pp, John Wiley & Sons.

[25] At variance with the metal complex, the central carbon atom is involved in the π delocalization by using two p_π rather than d_π orthogonal orbitals, but in any case the four axial π linkages are supported by one bonding electron each (four half axial linkages in total).

[26] a) T.-G. Ong, G. P. A. Yap, D. S. Richeson, *J. Am. Chem. Soc.* **2003**, *125*, 8100-8101; b) F. Montilla, A. Pastor, A. n. Galindo, *J. Organom. Chem.* **2004**, *689*, 993-996.

[27] a) T. Peddarao, A. Baishya, M. K. Barman, A. Kumar, S. Nembenna, *New J. Chem.* **2016**, *40*, 7627-7636; b) M. Findlater, N. J. Hill, A. H. Cowley, *Dalton Trans.* **2008**, 4419-4423.

[28] a) P. F. Kuijpers, J. I. van der Vlugt, S. Schneider, B. de Bruin, *Chem. Eur. J.* **2017**, *23*, 13819-13829; b) M. Goswami, V. Lyaskovskyy, S. r. R. Domingos, W. J. Buma, S. Woutersen, O. Troeppner, I. Ivanović-Burmazović, H. Lu, X. Cui, X. P. Zhang, E. J. Reijerse, S. DeBeer, M. M. van Schooneveld, F. F. Pfaff, K. Ray, B. de Bruin, *J. Am. Chem. Soc.* **2015**, *137*, 5468-5479; c) A. I. O. Suarez, H. Jiang, X. P. Zhang, B. de Bruin, *Dalton Trans.* **2011**, *40*, 5697-5705.

[29] a) J. T. Groves, *J. Chem. Educ.* **1985**, *62*, 928; b) D. Balcells, C. Raynaud, R. H. Crabtree, O. Eisenstein, *Chem. Commun.* **2008**, 744-746.

[30] J. P. Brand, J. Waser, *Chem. Soc. Rev.* **2012**, *41*, 4165-4179.

[31] a) N. Vujkovic, B. D. Ward, A. Maisse-François, H. Wadepohl, P. Mountford, L. H. Gade, *Organometallics* **2007**, *26*, 5522-5534; b) K. Kawakita, E. P. Beaumier, Y. Kakiuchi, H. Tsurugi, I. A. Tonks, K. Mashima, *J. Am. Chem. Soc.* **2019**, *141*, 4194-4198.

[32] The components are structurally unaffected by the interaction, but their almost null free energy balance of +0.5 kcal mol^{-1} implies an attraction due to the dispersion forces, which is counterbalanced by the ~+10 kcal mol^{-1} entropy term. For these reasons, no Transition State could be detected for **6m$_S$**.

[33] The -383.5 cm^{-1} value of the unique imaginary frequency corroborated N1-C1 as the proper reaction coordinate, given its opposite oscillations from the equilibrium.

[34] W.-L. Man, J. Xie, P.-K. Lo, W. W. Y. Lam, S.-M. Yiu, K.-C. Lau, T.-C. Lau, *Angew. Chem. Int. Ed.* **2014**, *126*, 8603-8606.

[35] A reduced bond order with respect to the original triple bond is corroborated by the computed IR 391 cm^{-1} red shift

[36] M. Harris, S. A. Brusey, A. Moore, Y. Ortin, H. Müller-Bunz, G. Manca, C. Mealli, M. J. McGlinchey, *ChemPlusChem* **2016**, *81*, 292-306.

[37] a) A. R. Thornton, S. B. Blakey, *J. Am. Chem. Soc.* **2008**, *130*, 5020-5021; b) A. R. Thornton, V. I. Martin, S. B. Blakey, *J. Am. Chem. Soc.* **2009**, *131*, 2434-2435.

[38] R. Hoffmann, *Angew. Chem. Int. Ed.* **1982**, *21*, 711-724.

[39] C. Mealli, D. M. Proserpio, *J. Chem. Educ.* **1990**, *67*, 399.

[40] E. Peréz-Carreño, P. Paoli, A. Ienco, C. Mealli, *Eur. J. Inorg. Chem.* **1999**, *1999*, 1315-1324.

[41] a) J. N. Harvey, R. Poli, K. M. Smith, *Coord. Chem. Rev.* **2003**, *238-239*, 347-361; b) J. N. Harvey, M. Aschi, *Faraday Discuss.* **2003**, *124*, 129-143.

[42] M. B. Smith, J. March in *Advanced Organic Chemistry: Reactions, Mechanisms, and Structure* (6th ed.), New York: Wiley-Interscience, 2007, ISBN 978-0-471-72091

[43] The total barrier starting from **8m$_S$** is +29.1 kcal mol^{-1}, given the initial cost of the **3aa$_{iso}$'** scission from the metal.

[44] a) G. Stefan, *J. Chem. Phys* **2006**, *124*, 034108; b) A. D. Becke, *J. Chem. Phys* **1993**, *98*, 5648-5652.

[45] M. J. Frisch, G. W. Trucks, H. B. Schlegel, G. E. Scuseria, M. A. Robb, J. R. Cheeseman, G. Scalmani, V. Barone, B. Mennucci, G. A. Petersson, H. Nakatsuji, M. Caricato, X. Li, H. P. Hratchian, A. F. Izmaylov, J. Bloino, G. Zheng, J. L. Sonnenberg, M. Hada, M. Ehara, K. Toyota, R. Fukuda, J. Hasegawa, M. Ishida, T. Nakajima, Y. Honda, O. Kitao, H. Nakai, T. Vreven, J. A. Jr. Montgomery, J. E. Peralta, F. Ogliaro, M. Bearpark, J. J. Heyd, E. Brothers, K. N. Kudin, V. N. Staroverov, R. Kobayashi, J. Normand, K. Raghavachari, A. Rendell, J. C. Burant, S. S. Iyengar, J. Tomasi, M. Cossi, N. Rega, J. M. Millam, M. Klene, J. E. Knox, J. B. Cross, V. Bakken, C. Adamo, J. Jaramillo, R. Gomperts, R. E. Stratmann, O. Yazyev, A. J. Austin, R. Cammi, C. Pomelli, J. W. Ochterski, R. L. Martin, K. Morokuma, V. G. Zakrzewski, G. A. Voth, P. Salvador, J .J. Dannenberg, S. Dapprich, A. D. Daniels, Ö. Farkas, J. B. Foresman, J. V.Ortiz, J.Cioslowski, D. J. Fox Gaussian 0.9, revision B.01; Gaussian, Inc.: Wallingford, CT, 2010

[46] a) V. Barone, M. Cossi, *J. Phys. Chem. A* **1998**, *102*, 1995-2001; b) M. Cossi, N. Rega, G. Scalmani, V. Barone, *J. Comput. Chem.* **2003**, *24*, 669-681.

[47] M. Dolg, H. Stoll, H. Preuss, R. M. Pitzer, *J. Phys. Chem.* **1993**, *97*, 5852-5859.

[48] G. A. Petersson, A. Bennett, T. G. Tensfeldt, M. A. Al-Laham, W. A. Shirley, J. Mantzaris, *J. Chem. Phys* **1988**, *89*, 2193-2218.

[49] A. Schäfer, C. Huber, R. Ahlrichs, *J. Chem. Phys* **1994**, *100*, 5829-5835.

[50] M. Tanno, S. Sueyoshi, S. Kamiya, *Chem. Pharm. Bull.* **1982**, *30*, 3125-3132.

Entry for the Table of Contents

FULL PAPER

The Ru(TPP)$(NAr)_2$–catalyzed *one-pot* formation of indoles from alkynes and aryl azides was analyzed by a synergic experimental/computational study. The reaction was effective for the synthesis of differently C_3-substituted indoles and the DFT investigation elucidates the energy costs as well as associated orbital and electronic evolutions of the reaction.

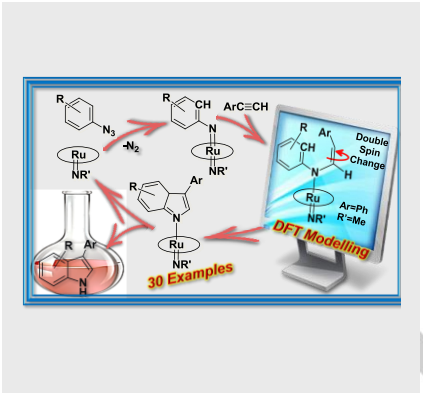

Daniela Intrieri, Daniela Maria Carminati, Paolo Zardi, Caterina Damiano, Gabriele Manca, Emma Gallo,* Carlo Mealli*

Page No. – Page No.

Indoles from Alkynes and Aryl Azides. Scope and Theoretical Assessment of Ruthenium Porphyrin-Catalyzed Reactions